Crystallite size dependence of thermoelectric performance of CuCrO2

Ngo, T. N. M.; Palstra, T. T. M.; Blake, G. R.

Published in:
RSC Advances

DOI:
10.1039/c6ra08035a

Publication date:
2016

RSC Advances

PAPER

View Article Online
View Journal | View Issue

Cite this: RSC Adv., 2016, 6, 91171

Crystallite size dependence of thermoelectric performance of $CuCrO_2$

T. N. M. Ngo,[ab] T. T. M. Palstra[a] and G. R. Blake*[a]

Received 28th March 2016
Accepted 18th September 2016

DOI: 10.1039/c6ra08035a

www.rsc.org/advances

The layered delafossite $CuCrO_2$ has attracted attention as a promising thermoelectric material because its electrical conductivity can be greatly increased by doping. Here we study the effect of crystallite size and morphology on the thermal conductivity, Seebeck coefficient and electrical resistivity, all important factors for thermoelectric performance. We have synthesized polycrystalline $CuCrO_2$ by three routes (solid state reaction, sol–gel method and hydrothermal synthesis), leading to samples with distinctly different particle sizes and morphologies. The smallest crystallites with a quasi-hexagonal shape of dimensions ~20 nm can be obtained by hydrothermal synthesis. These samples have the lowest thermal conductivity but their high resistivity dominates and has a detrimental effect on the thermoelectric figure of merit, *ZT*. Samples prepared by the sol–gel method exhibit relatively low thermal conductivity and resistivity and consequently the best *ZT*. We discuss the possibility of enhancing *ZT* further in this type of material.

1. Introduction

Cu-based delafossites $CuMO_2$, where M is a trivalent transition metal, first attracted attention for their p-type transparent conductivity. This offers potential applications in opto-electric devices, photo-electrochemical thin film catalysts for water splitting, steam reforming and gas purification.[1–3] The delafossite $CuCrO_2$ has a layered structure in which Cu layers alternate with layers of edge-shared CrO_6 octahedra. Both layers consist of two-dimensional triangular lattices. This can result in high electrical conductivities and high Seebeck coefficients, similar to $NaCoO_2$.[4,5] $CuCrO_2$ has received much interest in the search for new types of thermoelectric materials and the study of the origin of thermoelectric properties in these materials. Extensive studies have been carried out on both undoped and doped $CuCrO_2$, in which the Cr site can be doped with small concentrations of Mg, Ni, and Co ions to reduce the resistivity, especially Mg.[6–9] The decrease in electrical resistivity upon doping leads to an increased power factor (PF) $S^2\sigma$, where S is the Seebeck coefficient and σ is the electrical conductivity. Mg-doping improves the PF by an order of magnitude compared to the parent compound at room temperature, which reaches 1.4×10^{-4} W (m K^2)$^{-1}$ at 800 K.[10] Attempts have been made to reduce the electrical resistivity further by adding a co-dopant M′ including Zn, Ca, Ni and Co.[4] The highest value of figure of merit $ZT = 0.10$ is observed for the compound $CuCr_{0.97-x}Mg_{0.03}M'_xO_2$ with M′ = Ni and $x = 0.04$ at 1100 K, which is twice the value for samples only doped with Mg. Among other Cu-based delafossites, an improved PF of 7.10×10^{-4} W (m K^2)$^{-1}$ has been obtained for $CuRh_{0.9}Mg_{0.1}O_2$ over a broad temperature range between 400 and 1000 K.[11] The $CuFe_{1-x}Ni_xO_2$ series also exhibits high power factors, reaching 5.1×10^{-4} W (m K^2)$^{-1}$ for $x = 0.01$, which has a *ZT* of 0.14 at 1100 K.[8] However, all these Cu-based delafossites exhibit large thermal conductivities in the range 6–10 W (m K)$^{-1}$.[4,11] A reduction of thermal conductivity is therefore necessary to enhance the thermoelectric figure of merit.

The overall thermal conductivity κ of a material is the sum of the electronic and lattice components, κ_e and κ_{ph} respectively. For oxide materials in which the electrical conductivity is low, the thermal conductivity is strongly determined by the lattice component. Therefore, aiming to reduce the thermal conductivity implies decreasing the heat transport, notably by enhancing the phonon scattering. Approaches that have been used involve increasing the degree of atomic disorder by introducing point defects, utilizing resonant scattering by localized rattling atoms, and enhancing phonon scattering at interfaces by nanostructuring.[12–15] The density of interfaces can be increased by (i) reducing the grain size using different fabrication methods, (ii) partitioning a precursor phase in a thermodynamically stable product phase (such as thin rods of Sb in an InSb matrix), and (iii) fabricating low-dimensional structures such as nanotubes/nanowires and superlattice structures.[12,16–19]

There have been several reports in which tuning the grain size can improve thermoelectric performance. For example, reducing the grain size of polycrystalline $Si_{0.8}Ge_{0.2}$ from 100 μm

[a]Solid State Materials for Electronics, Zernike Institute for Advanced Materials, University of Groningen, Nijenborgh 4, 9747 AG Groningen, The Netherlands. E-mail: g.r.blake@rug.nl

[b]Department of Chemical Engineering, College of Engineering Technology, Can Tho University, Campus II, 3/2 Street, Ninh Kieu District, Can Tho City, Vietnam

to 1 μm reduced κ_{ph} by almost a factor of two.[20] A grain size reduction from 5 μm to 150 nm in the skutterudite $CoSb_3$ decreased κ_{ph} from ~4 W (m K)$^{-1}$ to ~1 W (m K)$^{-1}$ at 700 K.[21] Hot-pressed nanocrystals of $(Bi,Sb)_2Te_3$ with an average grain size of 20 nm showed a total thermal conductivity of 1.3 W (m K)$^{-1}$ compared to 2.2 W (m K)$^{-1}$ for bulk ingots.[22] In copper-based systems, the improvement of thermoelectric properties by nanostructuring has been reported for example in $Cu_2CdSnSe_4$ nanocrystals[23] and $Cu_{1.75}Te$ nanosheets.[24] As the $CuCrO_2$ system has been widely studied with respect to increasing the PF and thus *ZT* by doping mainly on the Cr^{3+} site to reduce the resistivity, it is useful to investigate whether the thermoelectric performance can be further improved by decreasing the thermal conductivity with smaller grain size. Here we use different synthesis methods to tune the grain size and morphology, and we discuss how this affects not only the thermal conductivity but also the other parameters that influence the thermoelectric figure of merit.

2. Experimental

2.1 Synthesis

Polycrystalline powder samples of $CuCrO_2$ were produced using three methods: solid state reaction, sol–gel and hydrothermal synthesis. For the solid state method, a stoichiometric mixture of CuO and Cr_2O_3 was calcined in air at 1200 °C for 12 hours. For the sol–gel method, $Cu(NO_3)_2 \cdot xH_2O$ and $Cr(NO_3)_3 \cdot yH_2O$ were used as the precursors, which were dissolved in distilled water with NaOH as the mineralizer. Citric acid or acetic acid was added to the mixture with a molar ratio of acid : cations = 2 : 1. The obtained foamy solid gel was crushed into powder and was then fired at 650–900 °C to remove the organic component and to crystallize the $CuCrO_2$ particles. In the hydrothermal synthesis, Cu_2O and $Cr(NO_3)_3 \cdot xH_2O$ were used as the reactants. $Cr(NO_3)_3 \cdot xH_2O$ was dissolved in water while Cu_2O was separately dissolved in NaOH (3 M). The concentration of Cu_2O was varied from 0.25–3 mmol l^{-1}. The mixture was transferred to a Teflon container which then was put into a steel bomb and sealed well. The bomb was heated in the furnace to 190–220 °C for 60 hours, after which it was cooled naturally to room temperature in the furnace. The mixture after reaction contained a powder with small particle size. It was washed with distilled water until the pH reached 7 and then washed with ethanol. The wet powder was dried in an oven at 120 °C.

2.2 Instrumentation

X-ray powder diffraction (XRPD) patterns were obtained with a Bruker D8 Advance diffractometer operating in Bragg–Brentano geometry with CuK_α radiation. The patterns were fitted using the GSAS software suite.[25] An X-ray profile fitting program (XFIT) was used to fit the individual diffraction peaks using pseudo-Voigt (PV) and split Pearson (PVII) functions. The morphology of the $CuCrO_2$ particles was imaged using a Philips XL-30 scanning electron microscope (SEM) integrated with an energy-dispersive X-ray spectroscopy analyser for qualitative and quantitative analysis of the elemental composition of the sample surface. A JEM 2010F transmission electron microscope (TEM), operating at an accelerating voltage of 200 kV, was used for visualization of the size and morphology of small grains. A Physical Property Measurement System (PPMS), in combination with Keithley 237, 236 source-measure units and HP 3458A and Agilent 3458A multimeters, was used for Seebeck coefficient and electrical resistivity measurement. A home-made thermal conductivity setup was designed for use with the PPMS, using a turbomolecular pump connected to the top flange of the sample chamber to minimize the heat loss by the residual gas. The measurement was performed using a one-thermometer, two-heater technique. Here the temperature difference is measured at the hot end of the sample when using two heater elements. These heaters are mounted at different distances from the thermal ground. The wiring was designed such that the heat loss of the wires was at most 5% of the thermal conduction to the thermal ground. The time dependence of the thermal response was analysed in order to eliminate a linear drift term from the exponential decay upon switching between the two heaters.

3. Results and discussion

3.1 Characterization

The synthesis of $CuCrO_2$ by solid state reaction (SS) is straightforward. Fig. 1a shows the fitted XRPD pattern, indicating a single delafossite phase with the 3R structure. The space group is $R\bar{3}m$ and the refined lattice parameters are a = 2.97528(5) Å, c = 17.107(3) Å at room temperature, which is consistent with other studies.[26–28] Using the sol–gel (SG) method, the powder obtained from the dried gel was heated further at various temperatures between 650 and 900 °C. Only samples heated above 850 °C were single phase; at lower temperature, diffraction peaks corresponding to CuO or Cu_2O and the spinel $CuCr_2O_4$ were observed. Fig. 1b shows the XRPD pattern of a SG powder heated at 850 °C. The peaks are broader than those of the SS sample. The majority phase corresponds to the 3R structure with preferred orientation along the [001] direction, as illustrated by the stronger 006 peak compared to the SS sample. Some weak extra peaks are also apparent (see inset of Fig. 1b) and probably correspond to the metastable 2H structure.[29] However, the peak positions are not exactly in agreement with the previously reported hexagonal structure with space group $P6_3/mmc$;[30] in our case it appears that the 2H phase undergoes a slight orthorhombic distortion to a unit cell with lattice parameters $a' \approx a$, $b' \approx b\sqrt{3}$, $c' \approx c$ where a = 2.9908(9) Å, b = 5.277(2) Å, c = 11.903(4) Å. This phase accounts for ~5 mol% of the sample. In the hydrothermal (HT) synthesis Cu_2O concentrations above 1.0 mmol l^{-1} and low synthesis temperatures of 180–200 °C resulted in samples containing CuO and other impurity phases with sharp diffraction peaks, although some $CuCrO_2$ was formed. When the synthesis was carried out at 210–220 °C with a Cu_2O concentration below 1.0 mmol l^{-1}, in most cases no sharp impurity peaks were observed. Fig. 1c shows the XRPD pattern of a powder sample obtained from this hydrothermal method. The broad peaks indicate very small grains and the pattern is similar to those previously

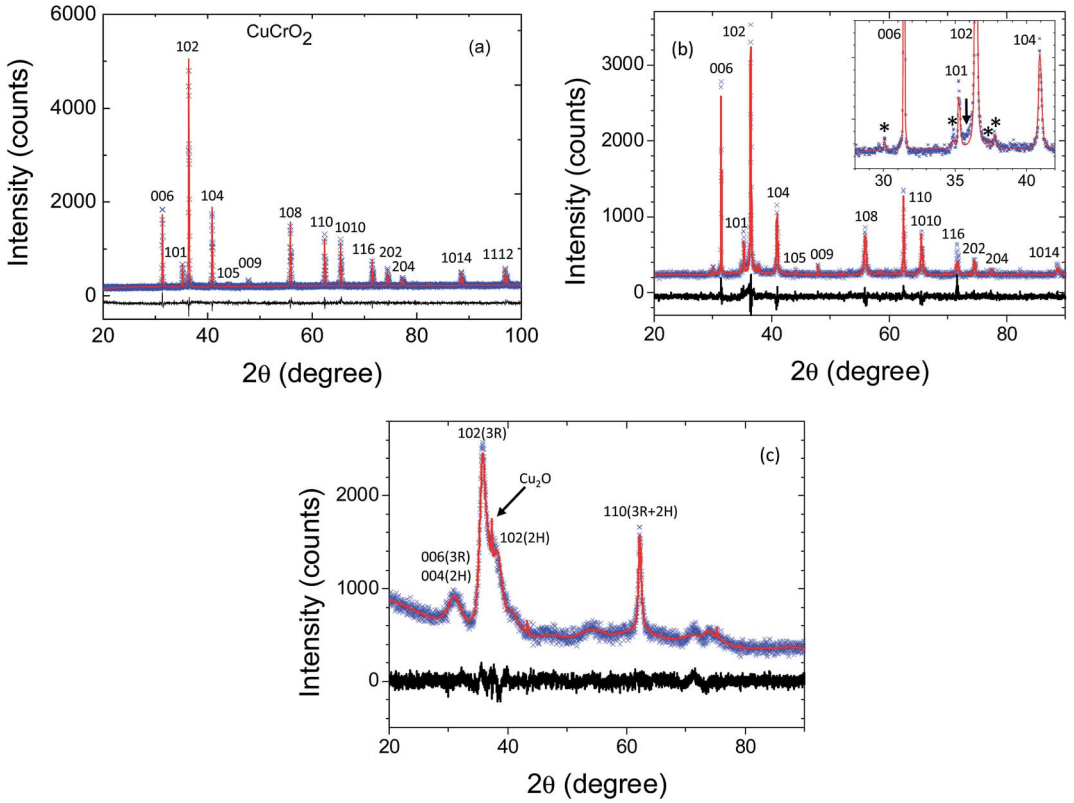

Fig. 1 Fitted XRPD patterns of $CuCrO_2$ powders synthesized by (a) solid-state reaction, (b) sol–gel method, and (c) hydrothermal method. The symbol * in (b) indicates peaks originating from a minority 2H phase and the arrow indicates a possible weak peak from a Cu_2O impurity.

reported for hydrothermally synthesized $CuCrO_2$.[29,31] Our as-synthesised samples contained a mixture of 2H and 3R phases, as shown by the splitting of the 102 peak into a broad doublet in Fig. 2, which presents the XRPD patterns of samples synthesized using various Cu_2O concentrations and temperatures. We notice that in general there is no observable difference between samples sintered at 210 or 220 °C. However, samples prepared with low Cu_2O concentrations sometimes contained CuO as an impurity, as evidenced by the sharp 11−1 and 111 peaks at ~35.7° and ~39.0° for the sample synthesized at 210 °C with 0.25 mmol Cu_2O. To verify that the main phase with broad peaks is $CuCrO_2$, the powder was further heated at 1050 °C to increase the grain size. Phase analysis then confirmed that the sample was single phase 3R-$CuCrO_2$; the 2H phase disappeared with annealing.

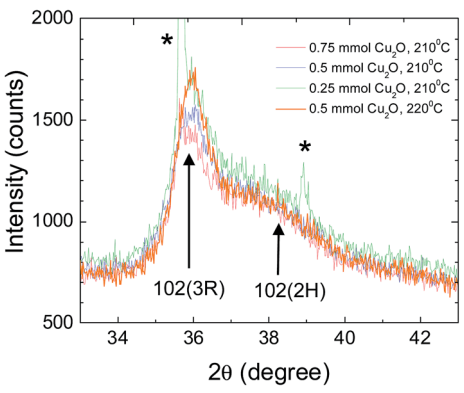

Fig. 2 Partial XRPD patterns of $CuCrO_2$ samples synthesized by the hydrothermal method at different Cu_2O concentrations and temperatures. The broad 102 peaks correspond to a mixture of 3R and 2H phases. Sharp peaks from a CuO impurity are indicated by the symbol *.

3.2 Particle size and morphology

Fig. 3 shows SEM images of $CuCrO_2$ particles synthesized using the three methods. The grain size of the samples from the SS and SG methods (Fig. 3a and b) ranges from 2–5 μm. The particles crystallize mainly in a hexagonal shape as expected for the delafossite structure.[2,4,10,32] For the HT sample synthesized with 0.25 mmol Cu_2O at 220 °C, in Fig. 3c, we observe that the grains have a round shape instead of the hexagonal shape observed for the other two methods. The grain size is smaller than 200 nm. The round shape and small grain size led to difficulties in pressing the powder into pellets for transport measurements as it was fluffy and light. When heated at 850 °C, the particles become hexagonal in shape although they are thin (Fig. 3d). For the $CuCrO_2$ powder synthesized at 210 °C with 0.75 mmol Cu_2O, the grain size is too small to be visible by SEM. The TEM image shown in Fig. 3e confirms the very small grain size of ~15 nm.

Due to the overlap of broad XRPD peaks for the hydrothermal samples, only the 110 peak at $2\theta \approx 62°$ was suitable for

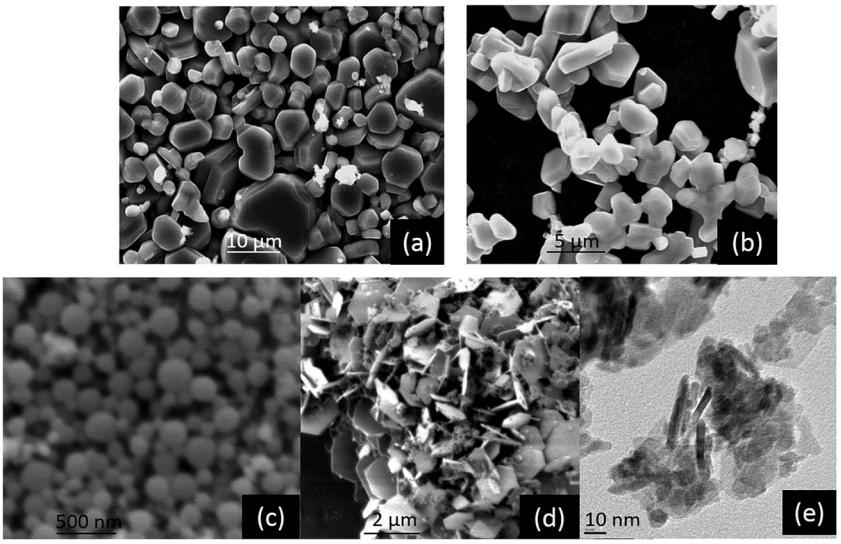

Fig. 3 SEM images of samples synthesized by (a) solid state reaction at 1200 °C, (b) sol–gel method at 850 °C, (c) hydrothermal method with 0.25 mmol Cu_2O at 220 °C and then (d) sintered at 850 °C, and (e) TEM image of sample synthesized by hydrothermal method with 0.75 mmol Cu_2O at 210 °C.

estimation of the average crystallite size D using the Scherrer formula[33]

$$D_{hkl} = \frac{k\lambda}{\beta \cos \theta} \quad (1)$$

where k is a constant ~1, λ is the X-ray wavelength, β is the full-width-at-half-maximum minus the instrumental peak width, and θ is the diffraction angle.

It should be noted that the 110 peak gives an estimate of the average crystallite size only in the *ab*-plane direction. Furthermore, fitting a single peak does not allow evaluation of possible peak broadening due to strain. Table 1 presents the average crystallite size calculation for $CuCrO_2$ samples from the three methods. As expected, the crystallite sizes of the SS and SG samples are biggest (>100 nm), as observed clearly in the SEM images where the grain sizes are several microns. We notice that the crystallite sizes obtained from XRPD for the HT samples are well below 20 nm, which is consistent with the TEM image in Fig. 3e. Similar calculated sizes that range between 20 and 38 nm have been reported elsewhere for the HT $CuCrO_2$ samples with similar broadened XRPD peaks.[29,34,35] Despite the fact that SEM is incapable of resolving the small size of these crystallites, the TEM image suggests that we indeed obtain nanocrystalline grains in the as-prepared HT $CuCrO_2$ samples. Various samples were sintered at high temperature to form pellets for transport measurements. The density was 80–85% for the SS samples and ~75% for the SG samples. Due to difficulties in pressing pellets from the hydrothermally synthesised powder, these samples had much lower densities of only ~45% for sample HT2-2 sintered at 1050 °C and ~65% for sample HT2-1 sintered at 1200 °C. Thus, the HT samples contain significant voids between the powder grains. Table 2 presents the grain sizes of the sintered samples estimated from SEM.

Table 1 Estimated average in-plane crystallite size D of $CuCrO_2$ determined by XRPD for samples synthesized by hydrothermal method (HT1–HT4), sol–gel method (SG1–SG2) and solid state reaction (SS1–SS2)

Sample	Conditions	2θ, deg.	FWHM (deg.)	D (nm)
HT1	0.75 mmol, 210 °C	61.52	0.66(2)	16
HT2	0.5 mmol, 210 °C	61.58	0.679(2)	15
HT3	0.5 mmol, 220 °C	61.63	0.58(2)	18
HT4	0.75 mmol, 220 °C	61.65	0.59(2)	17
SG1	Acetic acid, 850 °C, 10 h	62.36	0.07(1)	>100
SG2	Citric acid, 850 °C, 10 h	62.41	0.06(1)	>100
SS1	SS, 1000 °C, 10 h	62.41	0.09(1)	>100
SS2	SS, 1200 °C, 12 h	62.41	0.07(1)	>100

3.3 Electrical resistivity

$CuCrO_2$ is reported to be a p-type semiconductor, thus, the electrical resistivity decreases with increasing temperature.[10,36–38] Fig. 4a shows that this behaviour is observed for all our $CuCrO_2$ samples. The resistivity of the SS sample at 300 K is ~10 Ω m, consistent with that reported in the literature.[37] The SG method reduces the resistivity by an order of magnitude compared to the SS sample, while the HT synthesis increases the resistivity by an order of magnitude. The resistivity of the SG1-1 sample (sintered at 1100 °C) is higher than that of the

Table 2 Grain size d from SEM for sintered $CuCrO_2$ samples

Sample	Sintering temperature (°C)	d (μm)
HT2-1	1200	1
HT2-2	1050	<1
SS	1200	2–5
SG1-1	1100	10
SG1-2	1200	>10

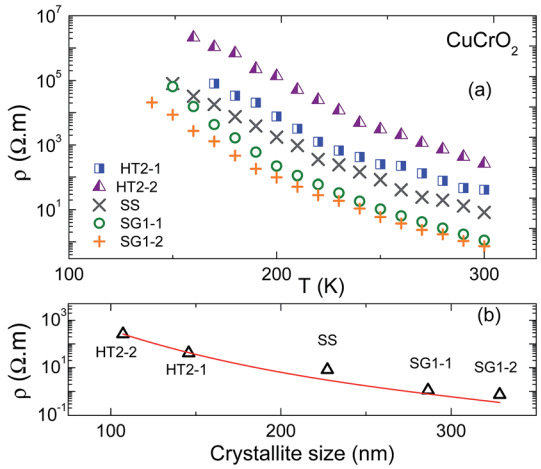

Fig. 4 (a) Electrical resistivity of different $CuCrO_2$ samples as a function of temperature. (b) Room temperature resistivity *versus* crystallite size.

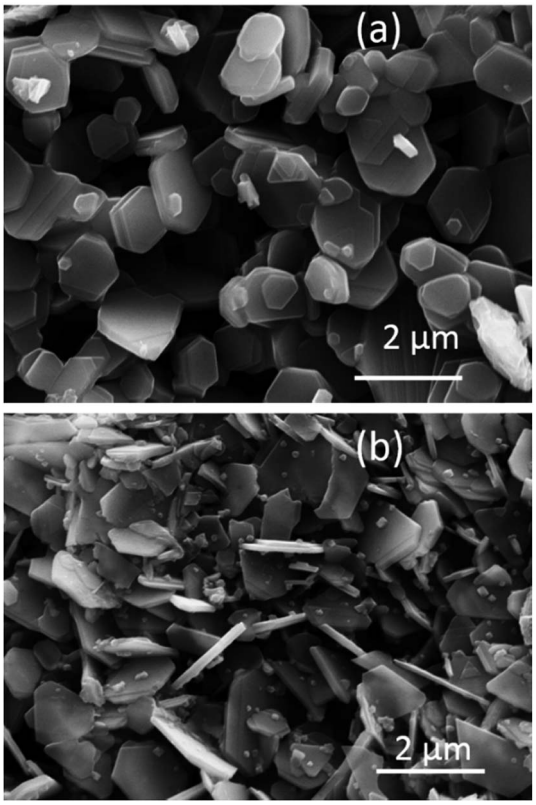

Fig. 5 SEM images of (a) sample HT2-1 sintered at 1200 °C and (b) HT2-2 sintered at 1050 °C.

SG1-2 sample (sintered at 1200 °C). This can be explained by the larger grain size of SG1-2 with fewer grain boundaries. Similarly, the sample HT2-2 (sintered at 1050 °C) has higher resistivity than HT2-1 (sintered at 1200 °C) not only due to grain size but also because HT2-2 is much less dense. The morphology of the grains of the SG samples is different from that of the other samples as the particles are more connected to each other when the sample is calcined at 850 °C, as apparent in Fig. 3b. At this relatively low temperature, the grain boundaries are thus more limited in number. When the powder is pressed and sintered at higher temperature, the grains grow easily with a reduction in the number of grain boundaries. However, if the sintering is performed at the relatively low temperature of 1000 °C, the sample is very fragile to handle. This is the reason why the samples were sintered at 1100 °C and 1200 °C, although such high temperatures lead to larger grains without maintaining the hexagonal shape as in other samples. In the case of the HT method, increasing the sintering temperature also leads to a decrease in resistivity. SEM images (Fig. 5) reveal that the inhomogeneity in the grain sizes and grain orientations is reduced at higher sintering temperature. Obvious boundaries are still observed between the grains. Fig. 4b presents the crystallite size dependence of the resistivity at 300 K, which clearly indicates that a lower resistivity is observed for samples with larger crystallite size and fewer boundaries between the grains. These results also imply that the grain size has a greater influence on resistivity than the density, since the SS sample was significantly denser than the SG samples but has higher resistivity.

The activation energies E_a were calculated from the Arrhenius equation expressing the relation between the electrical conductivity ρ and temperature T: $\ln(\rho) = \rho_0 \exp(-E_a/kT)$, where ρ_0 is the pre-factor and k is Boltzmann's constant. The fitted E_a of the SS sample is 0.27 eV, which is in good agreement with literature.[7,10,39] The fitted activation energies of the samples SG1-1, SG1-2, HT2-1 and HT2-2 are 0.28, 0.24, 0.26 and 0.25 eV, respectively. We conclude that the activation energies do not noticeably vary with the grain size, even though the resistivity can be modified by more than an order of magnitude. This indicates that the grain size reduction process does not change the nature of the conduction but rather the pre-factor of the Arrhenius equation. This suggests that the current path has been changed. In HT2-2 (sintered at 1050 °C), the small and thin grains (hexagonal flakes) orient in different directions as observed in Fig. 3d. This may reduce the current flow, resulting in a higher resistivity. We note that doping can lead to significant changes in the activation energy because it influences the carrier density and mobility as well as the nature of the conduction. Mg-doped $CuCrO_2$ exhibits a decrease in E_a from 0.28 eV to 0.17 eV when the doping level is 2%.[7] The change in activation energy in this case originates from 3D variable range hopping in the doped sample which exhibits power law behaviour $\ln(\rho) \propto (1/T)^{1/4}$.[10] We conclude that in our undoped case, the resistivity is mostly determined by the grain size and the geometry of how the grains are connected.

3.4 Seebeck coefficient and power factor

Fig. 6 shows the Seebeck coefficient as a function of temperature and as a function of crystallite size at 300 K for five $CuCrO_2$ samples. These measurements are possible only above 150 K due to the high sample resistance with values larger than the input impedance of the voltmeter. Samples prepared by the HT method have the highest Seebeck coefficients of ~800 μV K^{-1} at

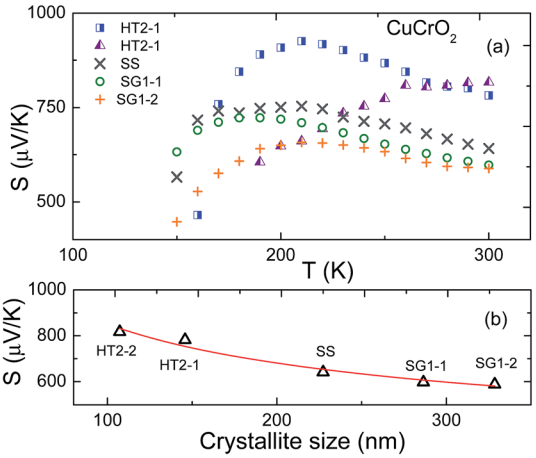

Fig. 6 Seebeck coefficient of different $CuCrO_2$ samples as a function of (a) temperature and (b) crystallite size at 300 K.

300 K. At room temperature, this is about 25% higher than those of other samples. The Seebeck coefficients of the SG samples are higher than that of the SS sample over most of the temperature range, but they are similar at 300 K. The Seebeck coefficient of the SS sample in our measurement is significantly lower than the reported value of 1100–1200 μV K^{-1} between 250 and 300 K with similar resistivity.[7] However, our value of 641 μV K^{-1} at 300 K is almost double that reported in ref. 10 (350 μV K^{-1}), where the resistivity (2.75 Ω m) is a factor of 3 smaller than our measured value (8.2 Ω m). A more insulating material typically has a higher Seebeck coefficient than a more conducting material, which is in agreement with our results.

Since the resistivity of undoped $CuCrO_2$ is high, the resulting power factor (PF) is very low at room temperature. The variation of the Seebeck coefficients of the $CuCrO_2$ samples is small compared to the variation in their resistivities. Fig. 7a shows the temperature dependence of the PFs and Fig. 7b shows the dependence of the PF on crystallite size at 300 K. At 300 K, the PFs of HT2-1, HT2-2, SS, SG1-1, SG1-2 are 0.015, 0.003, 0.05, 0.32 and 0.47 μW $(m\ K^2)^{-1}$, respectively. The values for the SG samples are comparable with the reported value of 0.44 μW $(m\ K^2)^{-1}$.[10] The PF increases significantly with temperature for the SS and SG samples, consistent with a previous study up to ~900 K.[37] The HT samples have the smallest power factors, which increase slowly with increasing temperature. Due to the high resistivity of $CuCrO_2$ at room temperature and below, the suitability for thermoelectric applications is more favourable in the high temperature range, where the resistivity decreases rapidly while the high Seebeck coefficient is maintained, resulting in a better PF. By doping with Mg, the PF can be increased by about two orders of magnitude due to a reduction of the resistivity.[10] Among the Mg-doped delafossites, the highest reported PF is ~700 μW $(m\ K^2)^{-1}$ between 400 and 1000 K for $CuRh_{0.9}Mg_{0.1}O_2$.[11]

3.5 Thermal conductivity and figure of merit

Fig. 8a and b show the temperature dependence of the thermal conductivity between 50 and 300 K and the crystallite size dependence of the thermal conductivity of the $CuCrO_2$ samples at 300 K, respectively. At 300 K, the hydrothermal sample HT2-2 (sintered at 1050 °C) has a lower thermal conductivity of ~4 W $(m\ K)^{-1}$ than HT2-1 (sintered at 1200 °C) for which the thermal conductivity is ~8.2 W $(m\ K)^{-1}$. The thermal conductivity is consistent with the observation that sample HT2-1 has bigger crystallite size and fewer voids, which leads to better heat transfer through the grains. Sample HT2-2 had a density of only ~45%, thus the large number of voids decreases the thermal conductivity significantly. Samples SG1-1 and SS have similar thermal conductivity of ~8.8 W $(m\ K)^{-1}$. These values are in agreement with the previously reported thermal conductivities of $CuCrO_2$ and Mg-doped $CuCrO_2$ (synthesized by the solid-state method) at room temperature, which vary between 6.5 and 9.5 W $(m\ K)^{-1}$.[37] This study showed that the thermal conductivity of $CuCrO_2$ decreases slightly with increasing temperature from 300–900 K. Our current results imply that reducing the crystallite size leads to a decrease of the thermal conductivity as intended, but at the expense of increasing the resistivity.

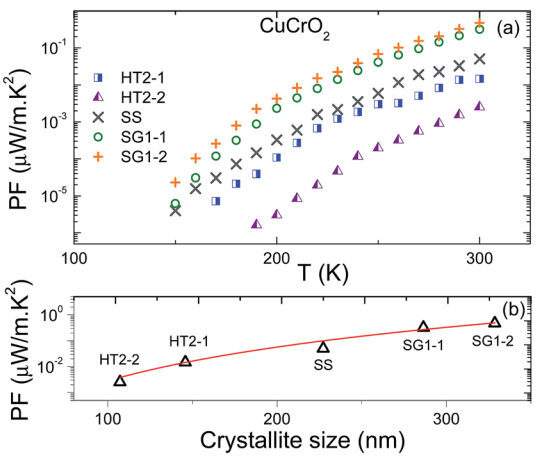

Fig. 7 Power factor (PF) of different $CuCrO_2$ samples as a function of (a) temperature and (b) crystallite size at 300 K.

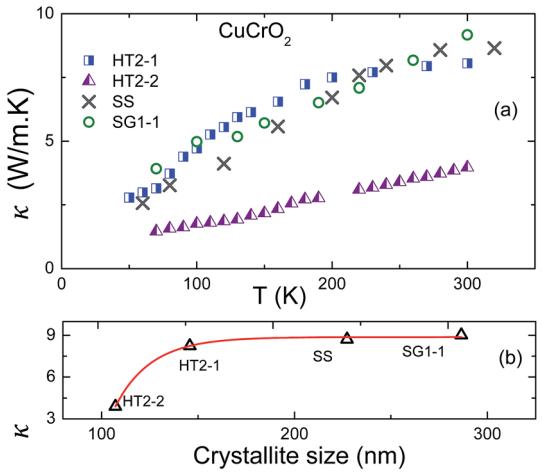

Fig. 8 Thermal conductivity of $CuCrO_2$ as a function of (a) temperature and (b) crystallite size at 300 K.

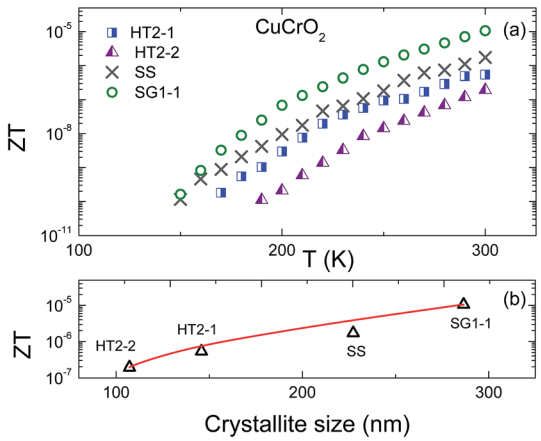

Fig. 9 Figure of merit *ZT* of different $CuCrO_2$ samples as a function of (a) temperature and (b) crystallite size at 300 K.

Fig. 9a and b present the figure of merit *ZT* of $CuCrO_2$ as a function of temperature and as a function of crystallite size at 300 K, respectively. As the resistivity of the HT samples is highest, their *ZT* values are relatively small. At 300 K, sample SG1-1 exhibits the best *ZT* of 1.1×10^{-5}, which is an order of magnitude higher than that of sample SS. The increasing trend of *ZT* with temperature for SG1-1 is steep and promising for better thermoelectric performance at higher temperatures. Extrapolating the SG1-1 curve, we may expect that *ZT* reaches ~0.01 at 1100 K. Although the thermal conductivity of $CuCrO_2$ decreases with decreasing crystallite and grain size, the corresponding increase in resistivity plays a more important role in determining *ZT*. If the resistivity could be reduced by doping with Mg, in particular for the SG sample, the PF and hence *ZT* might be enhanced for the $CuCrO_2$ system.

4. Conclusions

Hydrothermal (HT) synthesis allows the preparation of $CuCrO_2$ comprised of ~10 nm nanocrystallites. Samples synthesized using a sol–gel (SG) method consist of connected platelets of 5 μm across, whereas thick hexagonal grains of size ~10 μm with well-defined grain boundaries are obtained using solid state (SS) methods. Sintering results in significant grain growth for all the samples, where the small crystallites of the HT samples transform to thin hexagonal flakes of micron size and the SG samples exhibit less well-defined grain morphologies and boundaries. Smaller particle sizes lead to lower thermal conductivity as intended. However, the morphology, density of particle interfaces and orientation have a more dominant effect on the resistivity leading to a lower figure of merit *ZT* for the HT samples. Therefore, reducing the particle size of $CuCrO_2$ using the HT method is not advisable to enhance *ZT*. The SG synthesis route is more promising for optimizing the thermoelectric performance because it provides both low thermal conductivity and low electrical resistivity. If Mg-doping can successfully be carried out using SG synthesis, we can expect a reduction in the resistivity of about three orders of magnitude.[10,40] This can enhance the figure of merit of $CuCrO_2$ significantly.

Acknowledgements

The authors thank G. Li and G. ten Brink for the SEM and TEM images. We are grateful to J. Baas for his support with the thermal conductivity measurements. T. N. M. N. acknowledges the European Commission, EMA2 program, Lotus project 2010-2012 for financial support.

References

1 F. A. Benko and F. P. Koffyberg, *Mater. Res. Bull.*, 1986, **21**, 753–757.
2 H. Kawazoe, M. Yasukawa, H. Hyodo, M. Kurita, H. Yanagi and H. Hosono, *Nature*, 1997, **389**, 939–942.
3 S. Saadi, A. Bouguelia, A. Derbal and M. Trari, *J. Photochem. Photobiol., A*, 2007, **187**, 97–104.
4 K. Hayashi, K. Sato, T. Nozaki and T. Kajitani, *Jpn. J. Appl. Phys.*, 2008, **47**, 59–63.
5 I. Terasaki, Y. Sasago and K. Uchinokura, *Phys. Rev. B: Condens. Matter Mater. Phys.*, 1997, **56**, R12685–R12687.
6 M. Poienar, F. Damay, C. Martin, V. Hardy, A. Maignan and G. Andre, *Phys. Rev. B: Condens. Matter Mater. Phys.*, 2009, **79**, 014412.
7 A. Maignan, C. Martin, R. Frésard, V. Eyert, E. Guilmeau, S. Hébert, M. Poienar and D. Pelloquin, *Solid State Commun.*, 2009, **149**, 962–967.
8 T. Nozaki, K. Hayashi and T. Kajitani, *J. Chem. Eng. Jpn.*, 2007, **40**, 1205–1209.
9 S. Yanagiya, N. V. Nong, J. Xu and N. Pryds, *Materials*, 2010, **3**, 318–328.
10 T. Okuda, N. Jufuku, S. Hidaka and N. Terada, *Phys. Rev. B: Condens. Matter Mater. Phys.*, 2005, **72**, 144403.
11 A. Maignan, V. Eyert, C. Martin, S. Kremer, R. Frésard and D. Pelloquin, *Phys. Rev. B: Condens. Matter Mater. Phys.*, 2009, **80**, 115103.
12 C. Wan, Y. Wang, N. Wang, W. Norimatsu, M. Kusunoki and K. Koumoto, *Sci. Technol. Adv. Mater.*, 2010, **11**, 044306.
13 M. Yoshiya, M. Tada and T. Nagira, *Proc. Int. Symp. on Nano-Thermoelectrics*, 2007, 49.
14 B. C. Sales, D. Mandrus and R. K. Williams, *Science*, 1996, **272**, 1325–1328.
15 J. L. Cohn, G. S. Nolas, V. Fessatidis, T. H. Metcalf and G. A. Slack, *Phys. Rev. Lett.*, 1999, **82**, 779–782.
16 W. K. Liebmann and E. A. Miller, *J. Appl. Phys.*, 1963, **34**, 2653–2659.
17 A. I. Hochbaum, R. K. Chen, W. J. Liang, E. C. Garnett, M. Najarian, A. Majumdar and P. D. Yang, *Nature*, 2008, **451**, 163–167.
18 C. Chiritescu, D. G. Cahill, N. Nguyen, D. Johnson, A. Bodapati, P. Keblinski and P. Zschack, *Science*, 2007, **315**, 351–353.
19 D. L. Medlin and G. J. Snyder, *Curr. Opin. Colloid Interface Sci.*, 2009, **14**, 226–235.
20 C. B. Vining, W. Laskow, J. O. Hanson, R. R. V. D. Beck and P. D. Gorsuch, *J. Appl. Phys.*, 1991, **69**, 4333–4340.
21 J. L. Mi, T. J. Zhu, X. B. Zhao and J. Ma, *J. Appl. Phys.*, 2007, **101**, 054314.

22 B. Poudel, Q. Hao, Y. Ma, A. Minnich, B. Yu, X. Yan, D. Wang, A. Muto and D. Vashaee, *Science*, 2008, **320**, 634–638.
23 F. J. Fan, B. Yu, Y. X. Wang, Y. L. Zhu, X. J. Liu, S. H. Yu and Z. Ren, *J. Am. Chem. Soc.*, 2011, **133**, 15910–15913.
24 C. Nethravathi, C. R. Rajamathi, M. Rajamathi, R. Maki, T. Mori, D. Golberg and Y. Bando, *J. Mater. Chem. A*, 2014, **2**, 985–990.
25 B. H. Toby, *J. Appl. Crystallogr.*, 2001, **34**, 210–213.
26 K. Singh, B. Kundys, M. Poienar and C. Simon, *J. Phys. Condens. Matter*, 2010, **22**, 445901.
27 K. Kimura, H. Nakamura, K. Ohgushi and T. Kimura, *Phys. Rev. B: Condens. Matter Mater. Phys.*, 2008, **78**, 140401(R).
28 M. Poienar, V. Hardy, B. Kundys, K. Singh, A. Maignan, F. Damay and C. Martin, *J. Solid State Chem.*, 2012, **185**, 56–61.
29 M. Miclau, D. Ursu, S. Kumar and I. Grozescu, *J. Nanopart. Res.*, 2012, **14**, 1110.
30 O. Crottaz, F. Kubel and H. Schmid, *J. Solid State Chem.*, 1996, **122**, 247–250.
31 S. Zhou, X. Fang, Z. Deng, D. Li, W. Dong, R. Tao, G. Meng and T. Wang, *Sens. Actuators, B*, 2009, **143**, 119–123.
32 T. Kimura, J. Lashley and A. Ramirez, *Phys. Rev. B: Condens. Matter Mater. Phys.*, 2006, **73**, 220401.
33 A. L. Patterson, *Phys. Rev. B*, 1939, **56**, 978–982.
34 S. Zhou, X. Fang, Z. Deng, D. Li, W. Dong, R. Tao and G. Meng, *J. Cryst. Growth*, 2008, **310**, 5375–5379.
35 S. Zhou, X. Fang, Z. Deng, D. Li, W. Dong and R. Tao, *Sens. Actuators, B*, 2009, **143**, 119–123.
36 V. Eyert, R. Frésard and A. Maignan, *Chem. Mater.*, 2008, **20**, 2370–2373.
37 Y. Ono, K. Satoh, T. Nozaki and T. Kajitani, *Jpn. J. Appl. Phys.*, 2007, **46**, 1071–1075.
38 J. P. Doumerc, A. Wichainchai, A. Ammar, M. Pouchard and P. Hagenmuller, *Mater. Res. Bull.*, 1986, **21**, 745–752.
39 T. Okuda, Y. Beppu, Y. Fujii, T. Onoe, N. Terada and S. Miyasaka, *Phys. Rev. B: Condens. Matter Mater. Phys.*, 2008, **77**, 134423.
40 E. Guilmeau, M. Poeinar, S. Kremer, S. Marinel, S. Hébert, R. Frésard and A. Maignan, *Solid State Commun.*, 2011, **141**, 1798–1801.